

Trace Reconstruction with Language Models

Franziska Weindel¹, Michael Girsch¹, and Reinhard Heckel²

School of Computation, Information and Technology, Technical University of Munich
Munich Center for Machine Learning

July 18, 2025

Abstract

The general trace reconstruction problem seeks to recover an original sequence from its noisy copies independently corrupted by deletions, insertions, and substitutions. This problem arises in applications such as DNA data storage, a promising storage medium due to its high information density and longevity. However, errors introduced during DNA synthesis, storage, and sequencing require correction through algorithms and codes, with trace reconstruction often used as part of the data retrieval process. In this work, we propose TReconLM, which leverages language models trained on next-token prediction for trace reconstruction. We pretrain language models on synthetic data and fine-tune on real-world data to adapt to technology-specific error patterns. TReconLM outperforms state-of-the-art trace reconstruction algorithms, including prior deep learning approaches, recovering a substantially higher fraction of sequences without error.

1 Introduction

Trace reconstruction is a central problem in biological data analysis [Ant+20; BL+25; Org+18]. Given multiple noisy copies of a sequence (traces), the goal is to reconstruct the original sequence from as few traces as possible.

For example, in DNA data storage, the sequences to be reconstructed typically consist of 50-200 bases of adenine (A), cytosine (C), guanine (G), and thymine (T). For some sequences, as few as 2-10 noisy traces are available, each independently corrupted by insertions, deletions, and substitutions. However, existing trace reconstruction methods, including general algorithms such as MUSCLE [Edg04] and algorithms developed for DNA data storage [Qin+24], struggle when few traces are available and the error rates are high.

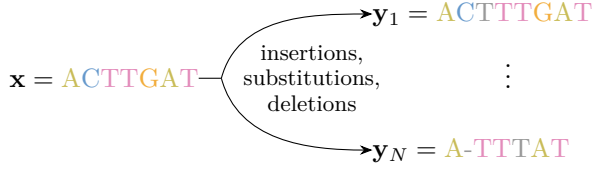
Existing trace reconstruction algorithms either assume a fixed error model [Sri+21; VS08] or rely on observed traces, often using dynamic programming techniques such as computing the longest common subsequence [Edg04; Gop+18; Sab+24]. Fixed error models fail to capture error dependencies observed in practice, such as error probabilities increasing with sequence length [Gim+23]. Relying only on observed traces ignores known error statistics, which can provide useful prior information, especially when few traces are available. These limitations motivate a data-driven approach that can be trained on synthetic data generated from an error model and fine-tuned on real-world data to capture observed error dependencies.

In this work, we frame the trace reconstruction problem for DNA data storage as a next-token prediction task and train decoder-only transformer models to generate sequence estimates from a set of traces. Our method, TReconLM (Trace Reconstruction with a Language Model), outperforms

¹Equal contribution. Emails: franziska.weindel@tum.de, michael.girsch@tum.de

²Email: reinhard.heckel@tum.de

Synthetic training data generation



Trace reconstruction as next-token prediction

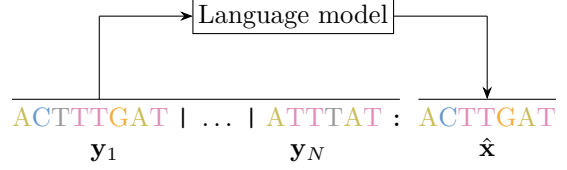


Figure 1: Left: Trace reconstruction aims to recover a sequence \mathbf{x} from N noisy copies \mathbf{y}_i , each corrupted by insertions, deletions, and substitutions. Right: We reformulate trace reconstruction as a next-token prediction task and train a transformer model to reconstruct \mathbf{x} from its noisy traces.

state-of-the-art methods for reconstructing DNA sequences from few traces. To address the lack of large-scale real data, we pretrain TReconLM on synthetic data and then fine-tune on data from existing DNA data storage systems to mitigate distribution shift and improve performance.

We additionally study scaling laws to understand how model size affects trace reconstruction performance. We find that in the considered regime, relatively small models (e.g., 38M parameters) perform best, and that increasing the model size further does not improve performance. We support this empirical finding with a theoretical analysis of trace reconstruction that explains the observed scaling behavior.

We make our code and models publicly available. Together, our results yield a new state-of-the-art method for efficient and accurate reconstruction of short traces. While our approach is conceptually simple, it is perhaps surprising that it outperforms both classical and prior neural network-based approaches (e.g., DNAformer [BL+25] and RobuSeqNet [Qin+24]) on a challenging algorithmic problem. This result highlights the potential of language models and next-token prediction as a tool for algorithm design.

2 Related work

Theoretical work on the trace reconstruction problem typically studies the minimum number of traces required to reconstruct a binary string corrupted by deletions with high probability [Bat+04; Cha21; DOS17; HL20; Hol+08]. However, perfect reconstruction from a small number of traces, which is the regime we focus on in this paper, is generally not possible.

Several trace reconstruction methods have been proposed in previous work. For traces corrupted by deletions, Batu et al. [Bat+04] introduced the bitwise majority alignment (BMA) algorithm, which uses symbol-wise majority voting. Viswanathan and Swaminathan [VS08] extended BMA for insertions, deletions, and substitutions, and Gopalan et al. [Gop+18] proposed another BMA-based approach.

Antkowiak et al. [Ant+20] performed trace reconstruction using multiple sequence alignment (MSA) with the MUSCLE algorithm [Edg04], followed by majority voting across alignment columns. Sabary et al. [Sab+24] proposed several dynamic programming-based methods, including shortest common supersequence and longest common subsequence algorithms. Their iterative algorithm (ITR) achieves state-of-the-art performance for trace reconstruction in DNA data storage. Srinivasavaradhan et al. [Sri+21] introduced TrellisBMA, which combines the BCJR algorithm [Bah+74] with BMA-based methods.

Qin et al. [Qin+24] proposed RobuSeqNet, a neural network-based approach that combines an attention mechanism, a conformer encoder, and an LSTM decoder. Input sequences are one-hot encoded, padded to a fixed length, and represented as matrices, which are then aggregated across traces. The attention module downweights misclustered sequences. On large clusters, RobuSeqNet performs slightly worse than the ITR algorithm [Sab+24].

Bar-Lev et al. [BL+25] proposed DNAformer, an end-to-end DNA data storage framework that includes a coding scheme and a transformer-based trace reconstruction model. Their neural architecture differs from ours in several key aspects. First, as in Qin et al. [Qin+24], input sequences are one-hot encoded. Second, the model uses a two-branch structure with shared weights, where one branch processes reversed input sequences. Third, DNAformer includes a learned alignment module, followed by a transformer encoder without positional embeddings or causal masks, and relies on postprocessing with dynamic programming. DNAformer achieves similar performance to the ITR algorithm [Sab+24].

Nahum et al. [NBTA21] proposed a sequence-to-sequence transformer for single-read trace reconstruction, where noisy sequences are grouped by length and processed by separate transformer networks. Their model effectively acts as a sequence classifier by mapping each noisy sequence to one of 256 predefined codewords. In contrast, our work uses next-token prediction instead of sequence-to-sequence mapping.

Dotan et al. [Dot+23] introduced BetaAlign, an encoder-decoder transformer for aligning biological sequences.

3 Background and problem statement

In this paper, we study the trace reconstruction problem. Given a set of noisy copies $\mathbf{y}_1, \dots, \mathbf{y}_N$ of a sequence \mathbf{x} , independently corrupted by unknown deletions, insertions, and substitutions, the goal is to compute a sequence estimate $\hat{\mathbf{x}}$ of the original sequence \mathbf{x} . Figure 1, left panel, illustrates the problem statement.

We focus on the trace reconstruction problem in DNA data storage, where the sequence \mathbf{x} is a DNA strand of length 50-200 bases that can be modeled as a random sequence over the quaternary alphabet. To motivate this setting, we briefly outline the DNA data storage pipeline.

In DNA data storage, digital information is first partitioned into short segments to accommodate current synthesis limitations, which prevent reliably writing long DNA strands. Each segment is then encoded using an error-correcting code and mapped to a DNA sequence $\mathbf{x}_i \in \{\text{A, C, T, G}\}^L$ of length L , resulting in a set $\mathcal{D} = \{\mathbf{x}_1, \dots, \mathbf{x}_M\}$. The sequences in \mathcal{D} are synthesized, amplified, and can be stored over long periods.

At readout, a subset of DNA sequences is sampled and sequenced, resulting in multiple unordered, noisy traces of the original sequences. The number of traces per sequence varies due to amplification bias and random sampling.

To recover the stored information, the first step is typically clustering, where the goal is to group traces originating from the same sequence \mathbf{x}_i . However, clustering is imperfect; a single original sequence can give rise to multiple clusters, and a single cluster can have traces from different original sequences [Ant+20; Org+18; Ras+17].

After clustering, the next step is to reconstruct a candidate sequence for each cluster. Given clusters containing $N \in \mathbb{N}_0$ noisy copies $\mathbf{y}_1, \dots, \mathbf{y}_N$ of a DNA sequence \mathbf{x} , each independently corrupted by unknown deletions, insertions, and substitutions, the goal is to compute cluster-wise

sequence estimates $\hat{\mathbf{x}}_i$ of the original sequences \mathbf{x}_i , which is the trace reconstruction problem defined at the beginning of this section.

We assume that the sequences \mathbf{x} consist of bases chosen uniformly at random over the alphabet $\{A, C, T, G\}$. This assumption is reasonable, as many existing DNA data storage systems randomize their sequences by adding a pseudorandom sequence, uniformly distributed over the four bases, to the input data before encoding [Ant+20; Org+18].

After trace reconstruction, a decoder typically corrects any remaining errors in the sequence estimates $\hat{\mathbf{x}}_i$, using the redundancy introduced during encoding to recover the original information.

4 Method

We formulate the trace reconstruction problem as a next-token prediction task and train a decoder-only transformer to solve it. Given a set of N traces

$$\mathcal{C} = \{\mathbf{y}_1, \dots, \mathbf{y}_N\},$$

we train a model f_{θ} with parameters θ to predict an estimate $\hat{\mathbf{x}}$ of the original sequence \mathbf{x} when prompted with the concatenation of traces

$$\mathbf{p} = \mathbf{y}_1 \mid \mathbf{y}_2 \mid \dots \mid \mathbf{y}_{N-1} \mid \mathbf{y}_N : . \quad (1)$$

We introduce the \mid token to concatenate traces and the $:$ token to mark the end of all traces. The model’s vocabulary is $\mathcal{V} = \{A, C, G, T, \mid, :, \#\}$, where $\#$ is the padding token.

Given prompt \mathbf{p} as in Equation (1), the model generates L tokens in an autoregressive manner via multiple forward passes. We use greedy decoding, selecting the most likely token at each step to obtain the final sequence estimate $\hat{\mathbf{x}}$. See Figure 1, right panel, for an illustration.

In Appendix B, we additionally consider alignment-based target representations (followed by majority voting to obtain a sequence estimate $\hat{\mathbf{x}}$), but find that directly predicting the sequence estimate $\hat{\mathbf{x}}$ performs best.

4.1 Training and data generation

We generate our synthetic data by first sampling an original sequence $\mathbf{x} \in \{A, C, G, T\}^L$ of length L uniformly at random from the set of all sequences. We then generate each trace \mathbf{y}_j by introducing, for each base in the original sequence \mathbf{x} , either a deletion, insertion, substitution, or no error, with probabilities p_D , p_I , p_S , and $p_T = 1 - p_D - p_I - p_S$, respectively. If a deletion is sampled, we append no base to trace \mathbf{y}_j and process the next base $x_{\ell+1}$. If an insertion is sampled, we append a random base chosen uniformly from the set $\{A, C, G, T\}$ to trace \mathbf{y}_j and reprocess the current base x_{ℓ} . If a substitution is sampled, we append a random base different from x_{ℓ} to trace \mathbf{y}_j and process the next base. If correct transmission is sampled, we append x_{ℓ} to trace \mathbf{y}_j and process the next base.

The traces $\mathbf{y}_1, \dots, \mathbf{y}_N$ are concatenated with the original sequence to form a training instance

$$\mathbf{y}_1 \mid \mathbf{y}_2 \mid \dots \mid \mathbf{y}_{N-1} \mid \mathbf{y}_N : \mathbf{x}. \quad (2)$$

We generate a large number of synthetic training examples (see Section 5.2 for details). For each training instance, we sample the error probabilities uniformly at random from the interval $[0.01, 0.1]$

and the number of traces N uniformly at random between 2 and 10, as this represents a practically relevant and challenging regime.

The transformer model is trained on the synthetic data by minimizing cross-entropy loss between the predicted sequence $\hat{\mathbf{x}}$ and the original sequence \mathbf{x} .

4.2 Finetuning on real data

In practice, error probabilities are often not independent and can, for example, vary with the position in the sequence [Ant+20]. This leads to a distribution shift between our synthetic training data and real-world data. To mitigate this shift, we fine-tune on two real-world datasets, the Noisy-DNA dataset [Ant+20] and the Microsoft dataset [Sri+21], as discussed in Sections 5.3.1 and 5.3.2, respectively.

From these datasets, we extract ground-truth sequences \mathbf{x} and associated noisy traces $\mathbf{y}_1, \dots, \mathbf{y}_N$, constructing training examples as given in Equation 2. We then fine-tune the model analogously to pretraining. Alternatively, fine-tuning or direct training on simulated data that better matches the characteristics of the respective channel is possible; however, this requires an accurate characterization of the DNA channel for the technology used, which is not necessarily straightforward.

5 Experiments

In this section, we evaluate the performance of our language model-based trace reconstruction method TReconLM. We focus on both synthetic data and datasets from existing DNA data storage systems. We find that TReconLM outperforms the state-of-the-art algorithm ITR [Sab+24] in the regimes we consider.

We measure performance using the following two metrics:

- **Levenshtein distance** $d_L(\mathbf{x}, \hat{\mathbf{x}})$: The minimum number of edits (deletions, insertions, and substitutions) required to transform the reconstructed sequence $\hat{\mathbf{x}}$ into the original sequence \mathbf{x} , normalized by the length L of the original sequence.
- **Failure rate**: The fraction of test instances in which the reconstructed sequence $\hat{\mathbf{x}}$ differs from the original sequence \mathbf{x} .

5.1 Baselines

We compare TReconLM to both dynamic programming-based and deep learning-based reconstruction methods. For dynamic programming-based methods, we consider the iterative algorithm (ITR) [Sab+24], trace reconstruction using MUSCLE [Edg04] with majority voting, TrellisBMA [Sri+21], BMALA [Gop+18], and VS [VS08]. For deep learning-based methods, we consider RobuSeqNet [Qin+24] and DNAformer [BL+25]. Hyperparameters and implementation details for all baselines are given in Appendix D.

In Appendix C.3 we also compare TReconLM to zero- and few-shot prompting of GPT-4o mini for trace reconstruction.

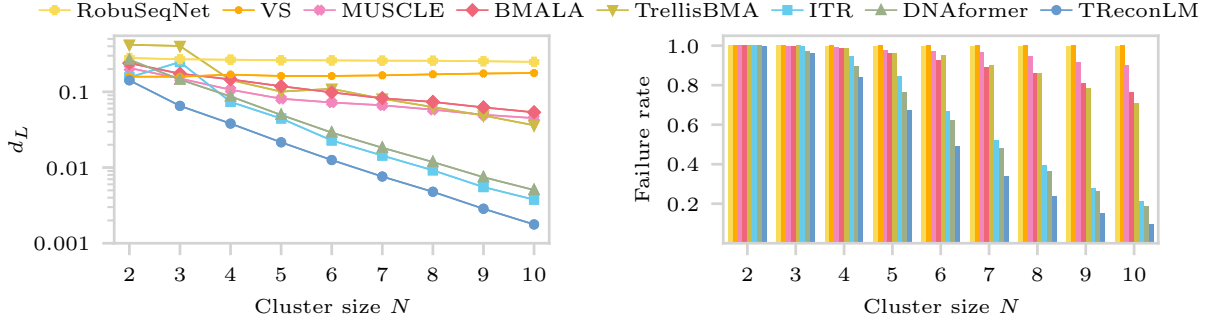


Figure 2: Average Levenshtein distances d_L and failure rates for synthetic data with sequence length $L = 110$. TReconLM achieves best performance in both metrics and across all cluster sizes.

5.2 Evaluation on synthetic data

We first evaluate reconstruction performance on synthetic data generated as described in Section 4.1 for three sequence lengths $L = 60, 110$, and 180 , which are representative of existing DNA data storage systems.

We train a decoder-only transformer model with $\sim 38\text{M}$ parameters on $\sim 300\text{M}$ examples ($\sim 440\text{B}$ tokens), totaling 1.0×10^{20} FLOPs. The model is trained over cluster sizes $N \in [2, 10]$, uniformly sampling N for each training instance. This gives only a small performance trade-off compared to training separate models for each cluster size (see Figure 3, right panel). We chose the model size based on the scaling law analysis in Section 5.4, which shows that increasing the number of parameters further does not improve performance.

We train our deep learning baselines, RobuSeqNet ($\sim 3\text{M}$ parameters) and DNAformer ($\sim 100\text{M}$ parameters), on the same training set. We do not match compute budgets as RobuSeqNet has a much smaller model size, and matching compute would require significantly longer training. However, in Appendix C, we show that TReconLM also outperforms RobuSeqNet when controlling for model size and DNAformer based on the performance reported in their original paper [BL+25].

We evaluate all reconstruction algorithms on a shared test set of 50K randomly generated examples, constructed in the same way as the training data. Each example is generated by first sampling a quaternary ground-truth sequence of length L uniformly at random and then independently introducing insertions, deletions, and substitutions at each position with error probabilities drawn uniformly from the interval $[0.01, 0.1]$.

Figure 2 shows the average Levenshtein distances and failure rates. TReconLM outperforms all baseline methods across all cluster sizes $N \in [2, 10]$ considered. Results for sequence lengths $L = 60$ and $L = 180$ are provided in Appendix A, showing that TReconLM also outperforms baseline methods on synthetic data for both shorter and longer sequences.

5.2.1 Generalization to higher noise levels and large cluster sizes

We next evaluate the robustness of TReconLM on traces with higher noise levels and under increasing cluster sizes.

We sweep over 10 noise levels by sampling insertion, deletion, and substitution probabilities from $\mathcal{U}(0.01 + 0.01k, 0.10 + 0.01k)$, where $\mathcal{U}(p_{\text{LB}}, p_{\text{UB}})$ denotes the uniform distribution over the

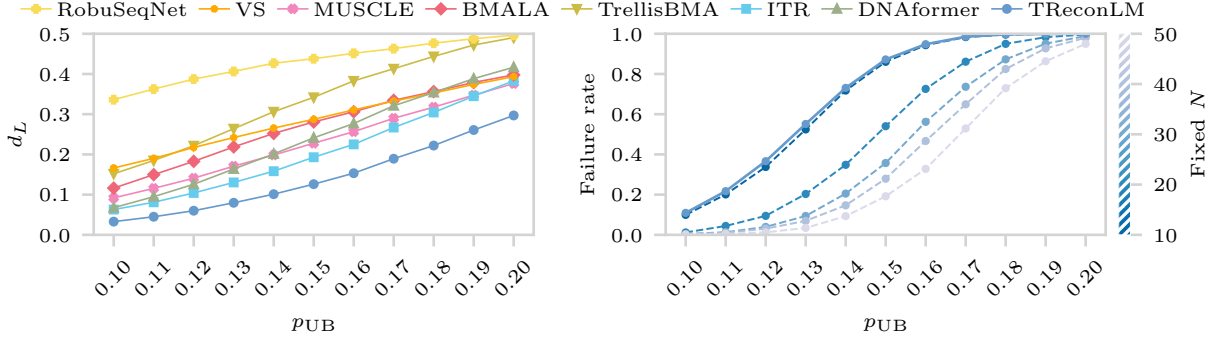


Figure 3: Left: Average Levenshtein distances d_L between reconstructed and ground-truth sequences under increasing noise levels. Right: Failure rates of TReconLM trained on fixed and larger cluster sizes and evaluated under increasing noise levels.

interval $[p_{LB}, p_{UB}]$. We use $k = 1, \dots, 10$, where $k = 0$ corresponds to the pretraining distribution $\mathcal{U}(0.01, 0.10)$, and $k = 10$ to $\mathcal{U}(0.11, 0.20)$.

Figure 3, left panel, shows the average Levenshtein distances between reconstructed and ground-truth sequences for TReconLM and baseline methods, evaluated on 5K randomly sampled test examples per noise level k . TReconLM can reconstruct sequences even under higher noise levels, outperforming the baselines despite a mismatch between training and test error distributions.

Figure 3, right panel, shows the failure rates of TReconLM across fixed and larger cluster sizes $N \in \{10, 20, 30, 40, 50\}$. For each cluster size, we train a separate model on the pretraining noise distribution $\mathcal{U}(0.01, 0.10)$ and evaluate it on 5K test sequences (of that cluster size) at each increased noise level k . All models are trained to reconstruct sequences of length $L = 110$ using a fixed compute budget of 1.0×10^{20} FLOPs. Increasing the cluster size from $N = 10$ to $N = 20$ improves reconstruction performance, with smaller gains at larger increases.

Figure 3, right panel, also compares a model pretrained on varying cluster sizes $N \in [2, 10]$ (solid line) to a model trained on a fixed cluster size $N = 10$ (dashed line), with both evaluated on 5K test sequences per noise level k . The results show only a small performance trade-off from training on varying cluster sizes.

5.3 Experiments on real data

In this section, we show that fine-tuning on real-world data improves reconstruction performance on the same dataset compared to using a pretrained model. We consider two datasets. The first is the Noisy-DNA dataset from Antkowiak et al. [Ant+20], which uses a cost-efficient writing technology at the expense of higher error probabilities. The second is the Microsoft dataset [Sri+21], which uses nanopore sequencing and similarly has high error probabilities. In both datasets, recovering the stored information is challenging, and trace reconstruction was originally used to reconstruct the data.

Fine-tuning on data from a single storage experiment results in a technology-adapted model that can be used for reconstruction in subsequent experiments with the same sequence length and read/write setup.

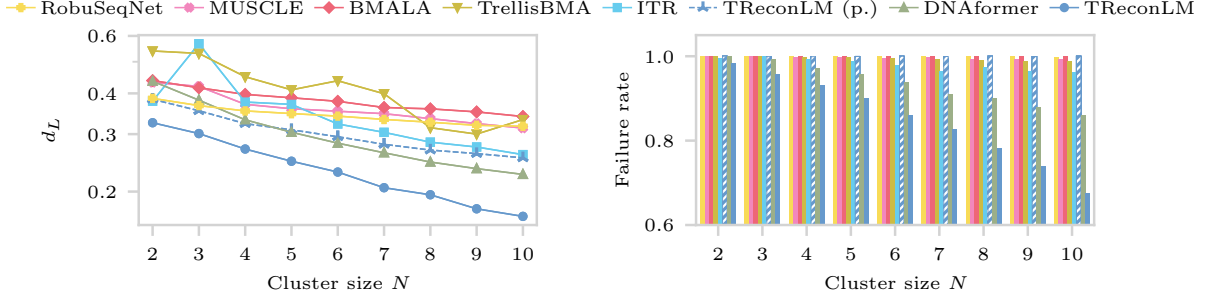


Figure 4: Average Levenshtein distances d_L and failure rates on the out-of-distribution Noisy-DNA dataset. The fine-tuned model achieves the lowest failure rates across all cluster sizes considered.

5.3.1 Real data experiment 1: Noisy-DNA dataset

The Noisy-DNA dataset [Ant+20] consists of $M = 16,383$ ground-truth sequences of length $L = 60$ bases and their unclustered traces. Estimated error probabilities are $p_I = 0.057$ (insertions), $p_D = 0.06$ (deletions), and $p_S = 0.026$ (substitutions), which are significantly higher than those in other DNA data storage systems [Gol+13; Gra+15; EZ17; Org+18].

Antkowiak et al. [Ant+20] report that error probabilities vary by position within the sequence, making this dataset well-suited for evaluating whether fine-tuning a model pretrained on synthetic data can adapt to real-world error statistics. For example, the insertion probability increases toward the end of the sequence, reaching up to $p_I = 0.3$, compared to the dataset-wide average of $p_I = 0.057$.

We construct our fine-tuning dataset by clustering traces by sequence index, discarding traces with index errors. This provides a simple and efficient clustering method. Although more advanced approaches (e.g., the similarity-based method from Zorita et al. [ZCF15]) could reduce failure rates, our goal is to compare the relative performance of reconstruction methods.

After clustering, we split the dataset into 80% train, 10% validation, and 10% test clusters. We divide clusters with more than ten traces into smaller subclusters to ensure that each example fits within our pretrained model’s context window.

For validation and test sets, we precompute fixed subclusters by repeatedly sampling a size between 2 and 10, then selecting that many traces without replacement until fewer than two remain, which are discarded. This yields 15,490 validation and 15,843 test examples.

During training, we apply the same sampling step but sample only one subcluster per example in each epoch, using the 12,910 train examples whose cluster size can exceed 10. Dynamically sampling subclusters increases training diversity by generating more combinations of noisy reads, effectively augmenting the data.

To prevent data leakage, we remove any traces in the train and validation sets that are too close to a ground-truth sequence in the test set, measured by Levenshtein distance. Given a sequence length $L = 60$ and estimated error probabilities $p_I = 0.057$, $p_D = 0.060$, and $p_S = 0.026$, the expected number of edit operations per trace is $L \times (p_I + p_D + p_S) = 8.58$. We set a conservative threshold and remove all traces from the train (30,109 of 720,635) and validation (3,861 of 91,267) sets whose Levenshtein distance to any test-set ground-truth sequence lies between 5 and 13, discarding any clusters with fewer than two remaining reads (2 in the training, 1 in the validation set).

For the non-deep learning baselines and our pretrained TReconLM model, we apply an additional preprocessing step to the test set that removes trailing C bases from all traces to improve performance.

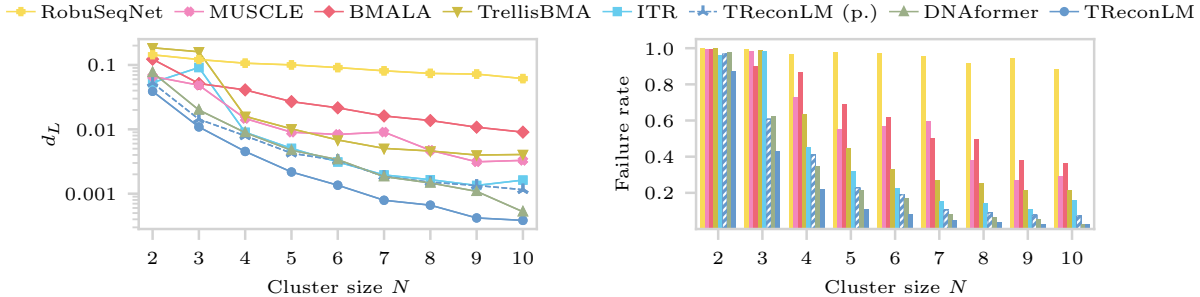


Figure 5: Average Levenshtein distances d_L and failure rates on the out-of-distribution Microsoft dataset. Both pretrained and fine-tuned TReconLM models outperform the considered baseline algorithms.

During library preparation, a C-rich tail is artificially added to each sequence for chemical reasons. Under normal conditions, this tail remains outside the typical 60-base sequencing window. However, a high deletion rate during synthesis can shift the C-rich tail into the window, making it visible in the traces. For fine-tuning, we do not apply this preprocessing step to allow the models to learn and adapt to the dataset’s error characteristics.

We fine-tune the pretrained TReconLM model and the deep learning baselines from Appendix A, all of which were trained on synthetic data to reconstruct sequences of length $L = 60$. TReconLM is fine-tuned using a compute budget of 1×10^{18} FLOPs, and the baselines are fine-tuned on the same dataset for an equivalent number of steps. See Table 1 for hyperparameters and training details for TReconLM, and Appendix D for the baselines.

Figure 4 shows the average Levenshtein distances and failure rates for different cluster sizes. The pretrained model fails to generalize to the technology-dependent error statistics. However, fine-tuning significantly improves performance, recovering 13% more sequences on average across cluster sizes compared to the state-of-the-art ITR algorithm.

5.3.2 Real data experiment 2: Microsoft dataset

We further evaluate the performance of TReconLM on the Microsoft dataset from Srinivasavaradhan et al. [Sri+21], which consists of $M = 10,000$ ground-truth sequences of length $L = 110$ and 269,707 traces. The traces are pre-clustered using the algorithm from Rashtchian et al. [Ras+17], with each cluster corresponding to a single ground-truth sequence. Estimated error probabilities are $p_I = 0.017$ (insertions), $p_D = 0.02$ (deletions), and $p_S = 0.022$ (substitutions).

As with the Noisy-DNA dataset [Ant+20], we split the data into 80% train, 10% validation, and 10% test clusters. Subclusters are precomputed for the validation and test sets and dynamically sampled during training to fit within the model’s context length. We obtain 5,062 and 5,235 examples for the validation and test sets, respectively, each with cluster sizes $N \leq 10$. For the train set, we obtain 7,976 examples with cluster sizes $N \in \mathbb{Z}$.

Figure 5 shows reconstruction performance after fine-tuning the TReconLM model from Section 5.2 using a compute budget of 1×10^{19} FLOPs. The deep learning baselines are fine-tuned on the same dataset as TReconLM for an equivalent number of steps. Both the pretrained and fine-tuned TReconLM models outperform all non-deep learning baselines, with the pretrained model matching the performance of the fine-tuned DNAformer, suggesting that TReconLM can generalize

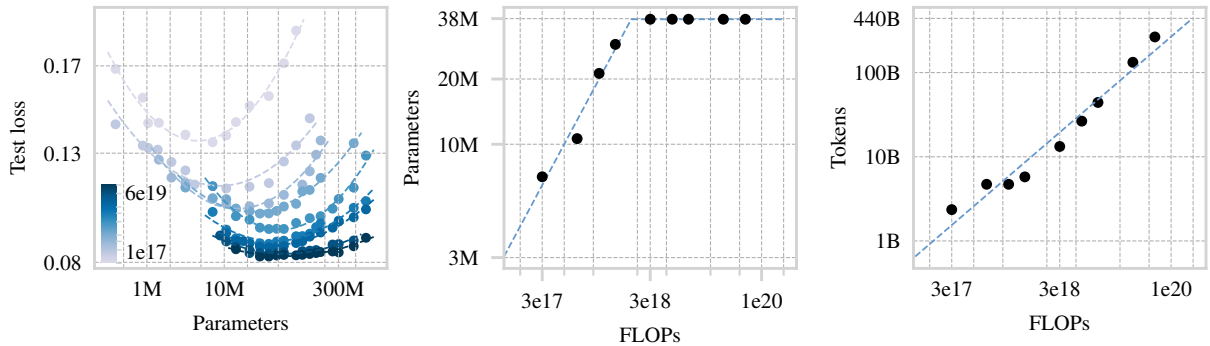


Figure 6: IsoFLOP curves for trace reconstruction. Left: Test loss for models ranging from 450K to 680M parameters, trained on sequences of length $L = 110$ across nine compute budgets from 10^{17} to 6×10^{19} FLOPs. Center: Number of parameters of the best-performing models versus compute, showing a plateau at high compute budgets. Right: Number of tokens versus compute, following scaling laws observed in language modeling.

to some extent from synthetic data to the Microsoft dataset, despite differences in error statistics.

5.4 Scaling Laws for trace reconstruction

We study how performance scales with compute and determine the best model size for reconstructing sequences of length $L = 110$ at a fixed compute budget. Following Approach 2 of Hoffmann et al. [Hof+22], we train a suite of models ranging from $N_p = 450K$ to 680M parameters at nine compute budgets $C \in \{1, 3, 6\} \times 10^{17,18,19}$ FLOPs, where each model is trained on $T = \frac{C}{6N_p}$ tokens.

We fix all optimization hyperparameters across runs, varying only the batch size (between 8 and $1.2K$) to match the compute budget, and scale the learning rate accordingly. The embedding dimension to depth ratio ranges from approximately 28 to 122. Other optimization hyperparameters are listed in Table 1 (Appendix A).

Figure 6, left panel, shows the IsoFLOP curves across the considered compute budgets, plotting test loss against model size (log scale). Under our hyperparameter settings, we observe that after a compute budget of 3×10^{18} FLOPs, the optimal model size plateaus at approximately 38M parameters (Figure 6, center panel). We provide a possible theoretical explanation for this behavior in Section 6. Figure 6, right panel, shows that the number of tokens processed versus compute follows a standard power law relationship.

6 Theory

We consider the following model to understand the scaling law behavior observed in Figure 6.

We consider a sequence $\tilde{\mathbf{x}} \in \{-1, 1\}^n$ and assume that we have m noisy copies of the sequence $\tilde{\mathbf{x}}_1, \dots, \tilde{\mathbf{x}}_m$, where each copy is obtained by independently flipping each of the entries in $\tilde{\mathbf{x}}$ with probability $p < 1/2$. Our goal is to estimate the sequence $\tilde{\mathbf{x}}$ based on the noisy copies. This is a special case of the trace reconstruction problem considered in this paper, where we only have substitutions, as opposed to substitutions, deletions, and insertions. Substitution errors are significantly simpler

than deletion and insertion errors, and since we know an optimal estimator for substitution errors we are able to analyze this setup.

We consider a linear estimator with $kn \leq mn$ many parameters for estimating each of the positions of \mathbf{x} . Without loss of generality we focus on estimating the first position of the sequence, $y = [\tilde{\mathbf{x}}]_1$. Our estimator takes the form:

$$\hat{y} = \text{sign} \left(\sum_{i=1}^k \mathbf{w}_i^T \tilde{\mathbf{x}}_i \right) = \text{sign}(\mathbf{w}^T \mathbf{x}).$$

The Bayes optimal estimator only uses the coordinates $[\tilde{\mathbf{x}}_1]_1, \dots, [\tilde{\mathbf{x}}_k]_1$ since the other coordinates are independent of $[\tilde{\mathbf{x}}]_1$, and is $\mathbf{w}_B = [1, 0, \dots, 1, 0, \dots, 1, 0, \dots]$ (or a scaled version thereof).

We consider a linear estimator with weights bounded by $\|\mathbf{w}\|_2 \leq B = \sqrt{kn}$ and we have $\|\mathbf{x}\|_2 \leq R = \sqrt{kn}$. We perform logistic regression to learn an estimator of the form $\text{sign}(\mathbf{w}^T \mathbf{x})$ from N examples. We consider the logistic regression estimate

$$\hat{\mathbf{w}} = \arg \min_{\mathbf{w}: \|\mathbf{w}\|_2 \leq B} \hat{R}(\mathbf{w}), \quad \text{where} \quad \hat{R}(\mathbf{w}) = \frac{1}{N} \sum_{i=1}^N \ell(\mathbf{w}^T \mathbf{x}_i, y_i), \quad (3)$$

where $\ell(z, y) = \log(1 + e^{-yz})$ is the logistic loss.

Proposition 1. With probability at least $1 - \delta$, the 0/1-error of the logistic regression estimate is bounded by

$$\mathbb{P} \left[\text{sign}(\hat{\mathbf{w}}^T \mathbf{x}) \neq y \right] \leq e^{-2k(1/2-p)^2} + \frac{1}{\sqrt{N}} \left(8BR + 6\sqrt{\log(2/\delta)/2} \right). \quad (4)$$

The proof of the proposition is in Appendix F. The first term in Equation 4 is (a bound on) the error of the Bayes optimal estimator with kn parameters. As the number of parameters increases (from k up to m) the error decreases. The second term is the error induced by learning this estimator based on N examples. The behavior in Figure 6 is consistent with such a bound. Once the model is sufficiently large, the first term in the bound is close to zero and does not significantly improve further by increasing the model size. The second term describes a power law in the number of training examples, N , which is what we also observe empirically.

7 Conclusion and limitations

In this work, we proposed a deep learning-based approach for trace reconstruction and validated it in the context of DNA data storage. Our method, TReconLM, achieves lower Levenshtein distances and failure rates than state-of-the-art methods across small cluster sizes and a wide range of noise levels on both synthetic and real-world data.

Such a learning-based approach to trace reconstruction is suitable whenever training data can be simulated, which is often the case, also beyond DNA data storage.

The main limitation of TReconLM over classical, non-deep learning based approaches is that it requires training data and can perform poorly if the test data is very different from the training data.

Acknowledgements

This work was funded by the European Union (DiDAX, 101115134). Views and opinions expressed are, however, those of the authors only and do not necessarily reflect those of the European Union or the European Research Council Executive Agency. Neither the European Union nor the granting authority can be held responsible for them.

Impact statement

The code is available at <https://github.com/MLI-lab/TReconLM>. Pretrained and fine-tuned models for sequence lengths $L = 60, 110$, and 180 are available on Hugging Face at <https://huggingface.co/ml-lab/TReconLM>. To support reproducibility, the test datasets used in our experiments are publicly available at https://huggingface.co/datasets/ml-lab/TReconLM_datasets.

References

- [Ant+20] P. L. Antkowiak, J. Lietard, M. Z. Darestani, M. M. Somoza, W. J. Stark, R. Heckel, and R. N. Grass. “Low cost DNA data storage using photolithographic synthesis and advanced information reconstruction and error correction”. In: *Nature Communications*. 2020.
- [Bah+74] L. Bahl, J. Cocke, F. Jelinek, and J. Raviv. “Optimal decoding of linear codes for minimizing symbol error rate (Corresp.)” In: *IEEE Transactions on Information Theory*. 1974.
- [BL+25] D. Bar-Lev, I. Orr, O. Sabary, T. Etzion, and E. Yaakobi. “Scalable and robust DNA-based storage via coding theory and deep learning”. In: *Nature Machine Intelligence*. 2025.
- [BJM06] P. L. Bartlett, M. I. Jordan, and J. D. McAuliffe. “Convexity, classification, and risk bounds”. In: *Journal of the American Statistical Association*. 2006.
- [Bat+04] T. Batu, S. Kannan, S. Khanna, and A. McGregor. “Reconstructing strings from random traces”. In: *SODA*. 2004.
- [Cha21] Z. Chase. “New lower bounds for trace reconstruction”. In: *Annales de l’Institut Henri Poincaré, Probabilités et Statistiques*. 2021.
- [DOS17] A. De, R. O’Donnell, and R. A. Servedio. “Optimal mean-based algorithms for trace reconstruction”. In: *Proceedings of the 49th Annual ACM SIGACT Symposium on Theory of Computing*. 2017.
- [Dot+23] E. Dotan, Y. Belinkov, O. Avram, E. Wygoda, N. Ecker, M. Albuquerque, O. Keren, G. Loewenthal, and T. Pupko. “Multiple Sequence Alignment as a Sequence-to-Sequence Learning Problem”. In: *The Eleventh International Conference on Learning Representations*. 2023.
- [Edg04] R. C. Edgar. “MUSCLE: Multiple sequence alignment with high accuracy and high throughput”. In: *Nucleic Acids Research*. 2004.

- [EZ17] Y. Erlich and D. Zielinski. “DNA Fountain enables a robust and efficient storage architecture”. In: *Science*. 2017.
- [Gim+23] A. L. Gimpel, W. J. Stark, R. Heckel, and R. N. Grass. “A digital twin for DNA data storage based on comprehensive quantification of errors and biases”. In: *Nature Communications*. 2023.
- [Gol+13] N. Goldman, P. Bertone, S. Chen, C. Dessimoz, E. M. LeProust, B. Sipos, and E. Birney. “Towards practical, high-capacity, low-maintenance information storage in synthesized DNA”. In: *Nature*. 2013.
- [Gop+18] P. S. Gopalan, S. Yekhanin, S. D. Ang, N. Jovic, M. Racz, K. Strauss, and L. Ceze. *Trace Reconstruction from Noisy Polynucleotide Sequencer Reads*. U.S. Patent Application 15/536,115. 2018.
- [Gra+15] R. N. Grass, R. Heckel, M. Puddu, D. Paunescu, and W. J. Stark. “Robust chemical preservation of digital information on DNA in silica with error-correcting codes”. In: *Angewandte Chemie International Edition*. 2015.
- [Hof+22] J. Hoffmann, S. Borgeaud, A. Mensch, E. Buchatskaya, T. Cai, E. Rutherford, D. d. L. Casas, L. A. Hendricks, J. Welbl, A. Clark, et al. “Training compute-optimal large language models”. In: *arXiv:2203.15556*. 2022.
- [HL20] N. Holden and R. Lyons. “Lower bounds for trace reconstruction”. In: *The Annals of Applied Probability*. 2020.
- [Hol+08] T. Holenstein, M. Mitzenmacher, R. Panigrahy, and U. Wieder. “Trace reconstruction with constant deletion probability and related results”. In: *Proceedings of the Nineteenth Annual ACM-SIAM Symposium on Discrete Algorithms*. 2008.
- [Kar25] A. Karpathy. *nanoGPT*. <https://github.com/karpathy/nanoGPT>. GitHub repository. 2025.
- [NBTA21] Y. Nahum, E. Ben-Tolila, and L. Anavy. “Single-read reconstruction for DNA data storage using transformers”. In: *arXiv:2109.05478*. 2021.
- [Org+18] L. Organick, S. D. Ang, Y.-J. Chen, R. Lopez, S. Yekhanin, K. Makarychev, M. Z. Racz, G. Kamath, P. Gopalan, B. Nguyen, et al. “Random access in large-scale DNA data storage”. In: *Nature biotechnology*. 2018.
- [Qin+24] Y. Qin, F. Zhu, B. Xi, and L. Song. “Robust multi-read reconstruction from noisy clusters using deep neural network for DNA storage”. In: *Computational and Structural Biotechnology Journal*. 2024.
- [Ras+17] C. Rashtchian, K. Makarychev, M. Racz, S. Ang, D. Jevdjic, S. Yekhanin, L. Ceze, and K. Strauss. “Clustering billions of reads for DNA data storage”. In: *Advances in Neural Information Processing Systems*. 2017.
- [Sab+24] O. Sabary, A. Yucovich, G. Shapira, and E. Yaakobi. “Reconstruction algorithms for DNA-storage systems”. In: *Scientific Reports*. 2024.
- [Sri+21] S. R. Srinivasavaradhan, S. Gopi, H. D. Pfister, and S. Yekhanin. “Trellis BMA: Coded Trace Reconstruction on IDS Channels for DNA Storage”. In: *2021 IEEE International Symposium on Information Theory (ISIT)*. 2021.

- [VS08] K. Viswanathan and R. Swaminathan. “Improved string reconstruction over insertion-deletion channels”. In: *Proceedings of the nineteenth annual ACM-SIAM symposium on Discrete algorithms*. 2008.
- [ZCF15] E. Zorita, P. Cuscó, and G. J. Filion. “Starcode: Sequence Clustering based on All-Pairs Search”. In: *Bioinformatics*. 2015.

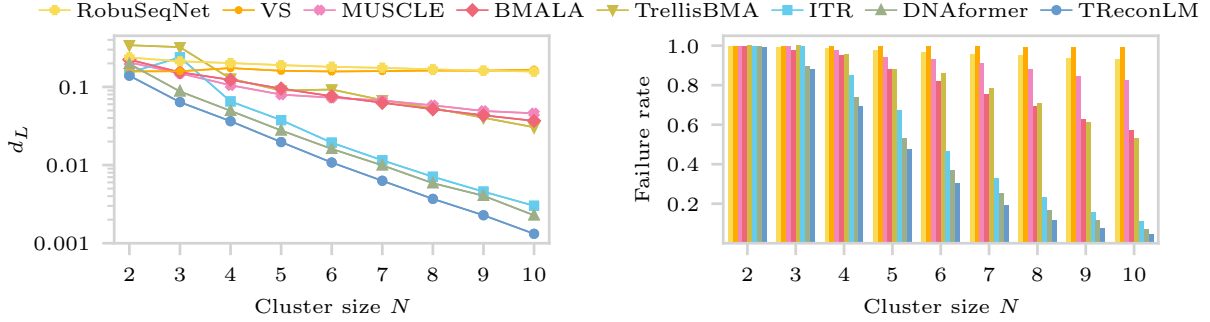


Figure 7: Average Levenshtein distances d_L and failure rates for in-distribution synthetic data with sequence length $L = 60$.

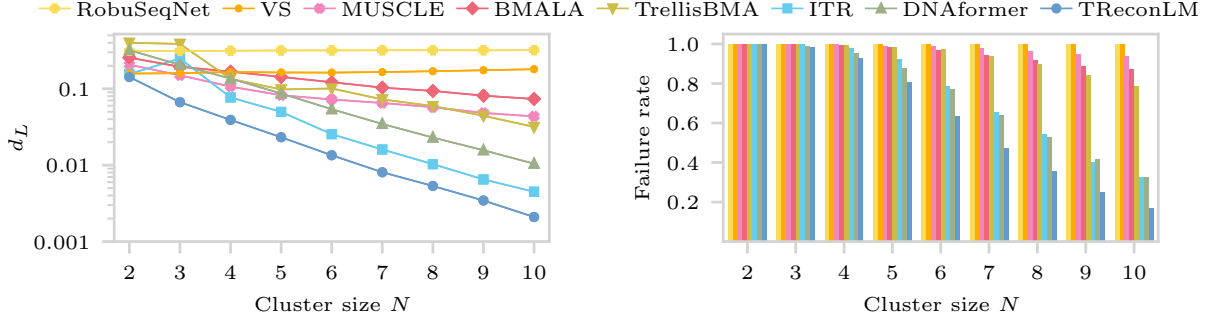


Figure 8: Average Levenshtein distances d_L and failure rates for in-distribution synthetic data with sequence length $L = 180$.

A Additional results for the IDS channel

Here, we additionally evaluate TReconLM’s performance on reconstructing sequences of length $L = 60$ and $L = 180$. We use the same model size of $\sim 38\text{M}$ parameters and the same compute budget of 1.0×10^{20} FLOPs as in Section 5.2. Both models are trained on $\sim 440\text{B}$ tokens. The number of training examples is adjusted based on the context length to match the fixed compute budget, with $\sim 551\text{M}$ examples for $L = 60$ and $\sim 184\text{M}$ examples for $L = 180$.

Optimization hyperparameters are listed in Table 1, largely following Karpathy [Kar25]. We apply gradient clipping with a maximum norm of 1.0. The learning rate is scaled based on batch size. The base learning rate is $1\text{e-}4$ for batch size 16, and we scale it proportionally to $\sqrt{\text{batch size}/16}$. We use a 5% warmup phase followed by cosine learning rate decay. For pretraining with a fixed cluster size and for fine-tuning, we use fixed learning rates ($1\text{e-}4$ and $1\text{e-}5$, respectively) without scaling based on batch size. Unless stated otherwise, we evaluate the checkpoint with the lowest validation loss.

Figure 7 shows Levenshtein distances and failure rates for sequence length $L = 60$. Figure 8 shows the corresponding results for sequence length $L = 180$. For both sequence lengths, TReconLM achieves lower Levenshtein distances and failure rates across all cluster sizes considered and outperforms the state-of-the-art reconstruction algorithm ITR [Sab+24] as well as other neural approaches [BL+25; Qin+24].

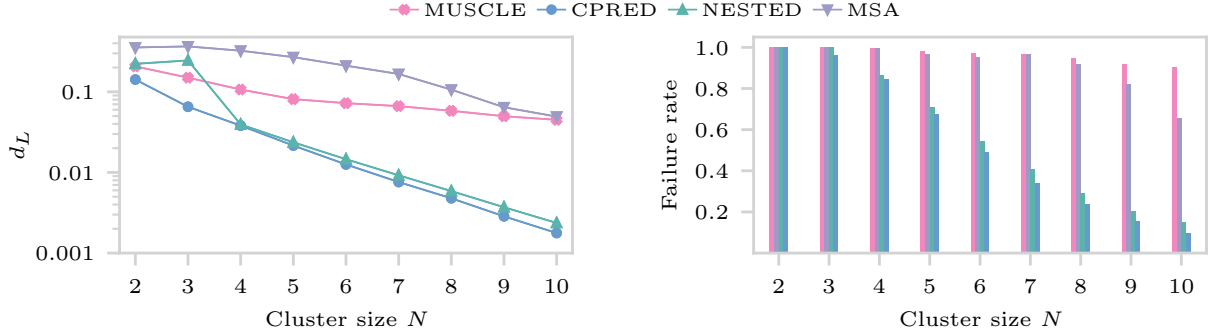


Figure 9: Comparison of different neural network targets. The candidate prediction target (CPRED) gives the lowest Levenshtein distances and failure rates.

Table 1: Optimization hyperparameters used during pretraining and fine-tuning.

Setting	Details	Batch	Iter.*	n_{emb}	n_{head}	n_{layers}	Adam β	Weight decay	LR	Dropout
Pretraining	$L = 60$	800	688,318	512	8	12	(0.9, 0.95)	0.1	7e-4	0.0
	$L = 110$	800	367,103	512	8	12	(0.9, 0.95)	0.1	7e-4	0.0
	$L = 180$	800	229,439	512	8	12	(0.9, 0.95)	0.1	7e-4	0.0
Fixed N	$N = 10$	800	367,103	512	8	12	(0.9, 0.95)	0.1	7e-4	0.0
	$N = 20$	512	315,368	512	8	12	(0.9, 0.95)	0.1	1e-4	0.1
	$N = 30$	256	383,260	512	8	12	(0.9, 0.95)	0.1	1e-4	0.2
	$N = 40$	256	311,503	512	8	12	(0.9, 0.95)	0.1	1e-4	0.2
	$N = 50$	256	263,579	512	8	12	(0.9, 0.95)	0.1	1e-4	0.2
Finetuning	Noisy DNA	8	685,307	512	8	12	(0.9, 0.95)	0.1	1e-5	0.3
	Microsoft	52	566,046	512	8	12	(0.9, 0.95)	0.1	1e-5	0.1

* Iterations are chosen to meet a fixed compute budget for each experiment.

B Multiple sequence alignment target

In this section, we evaluate different neural network targets for the trace reconstruction problem. As proposed by Dotan et al. [Dot+23], we can train a model f_{θ} to learn the alignment of the traces. For N traces $\mathbf{y}_1, \dots, \mathbf{y}_N$, one training instance is formed as

$$\mathbf{y}_1 \mid \mathbf{y}_2 \mid \dots \mid \mathbf{y}_{N-1} \mid \mathbf{y}_N : \text{MSA}(\mathbf{y}_1, \mathbf{y}_2, \dots, \mathbf{y}_{N-1}, \mathbf{y}_N) \#.$$
 (5)

The vocabulary for the alignment task is given by

$$\mathcal{V}_{\text{MSA}} = \{A, C, T, G, \mid, :, -, \#\},$$
 (6)

where we have an additional deletion token $-$ to achieve a column-wise matching of the aligned traces. For pretraining, we know the positions of deletions, insertions, and substitutions and construct the correct sequence alignment. During inference, we prompt the model with input \mathbf{p} (Equation (1)) and generate alignment tokens one by one until the padding token $\#$.

To obtain the sequence estimate $\hat{\mathbf{x}}$, we arrange the aligned traces $\hat{\mathbf{y}}_1, \dots, \hat{\mathbf{y}}_N$, each of length

L_{MSA} , as rows in a matrix:

$$\begin{array}{c|c|c|c|c}
 \hat{y}_{1,1} & \hat{y}_{1,2} & \cdots & \hat{y}_{1,L_{\text{MSA}}-1} & \hat{y}_{1,L_{\text{MSA}}} \\
 \hline
 \hat{y}_{2,1} & \hat{y}_{2,2} & \cdots & \hat{y}_{2,L_{\text{MSA}}-1} & \hat{y}_{2,L_{\text{MSA}}} \\
 \hline
 \vdots & & \vdots & & \vdots \\
 \hline
 \hat{y}_{N,1} & \hat{y}_{N,2} & \cdots & \hat{y}_{N,L_{\text{MSA}}-1} & \hat{y}_{N,L_{\text{MSA}}}
 \end{array} \tag{7}$$

We then compute $\hat{\mathbf{x}}$ by performing a column-wise majority vote over the aligned traces. The j -th entry of the estimated sequence $\hat{\mathbf{x}}$ can be calculated as

$$\hat{x}_j = \arg \max_{a \in \{A,C,T,G\}} \sum_{i=1}^N \mathbf{1}(\hat{y}_{i,j} = a), \tag{8}$$

where $\mathbf{1}(\cdot)$ denotes the indicator function.

We evaluate the following targets for the trace reconstruction: candidate prediction (CPRED) as described in Section 4, the MSA target as given in Equation (5) and a NESTED alignment target, where we perform a token-wise nesting of the ground-truth alignment $\text{MSA}(\mathbf{y}_1, \dots, \mathbf{y}_N)$. All deep learning models are trained under a fixed compute budget of 1.0×10^{20} FLOPs. We also evaluate MUSCLE to compare neural network-based alignment to dynamic programming-based alignment.

Figure 9 shows reconstruction distances for all target types. The candidate prediction (CPRED) target achieves the best overall performance. In contrast, alignment-based targets require longer context lengths and cannot be used for fine-tuning, as ground-truth alignments are generally unavailable for real-world data.

C Additional comparisons

Here, we provide additional comparisons to RobuSeqNet, DNAformer, and GPT-4o mini.

C.1 RobuSeqNet

We compare the performance of TReconLM to RobuSeqNet [Qin+24] when controlling for model size and compute. RobuSeqNet is a small model with $\sim 3\text{M}$ parameters and uses an LSTM decoder with a hidden dimension of 256. We train a TReconLM model with the same hidden dimension and total parameter count ($\sim 3\text{M}$), using the same compute budget (6×10^{17} FLOPs) and training dataset ($\sim 21\text{M}$ examples).

Figure 10, left panel, shows results for sequence length $L = 110$, evaluated on 50K test examples (identical to the test set used in Figure 2 of the main paper, where we did not control for model size). TReconLM also outperforms RobuSeqNet when controlling for model size and compute.

C.2 DNAformer

We compare the self-reported performance of DNAformer [BL+25], trained on synthetic data and evaluated on the Microsoft dataset with up to 16 reads per example, to that of TReconLM. For a fair comparison, we evaluate our pretrained TReconLM (input length $L = 110$) and recluster the noisy reads by index, as in Bar-Lev et al. [BL+25]. Since the Microsoft dataset lacks explicit indices, we follow their approach and use the shortest unique prefix of each ground-truth sequence as an

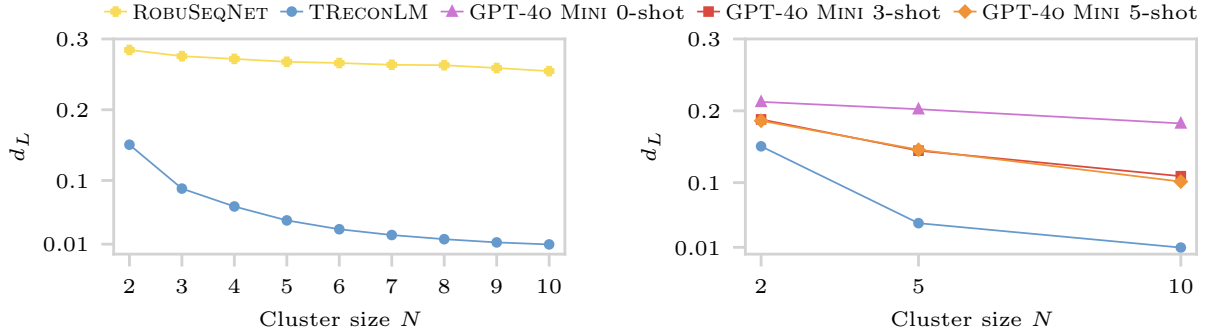


Figure 10: Left: Comparison of TRECONLM and RobuSeqNet at equal model size and compute for ground-truth sequence length $L = 110$ and cluster sizes $N \in [2, 10]$. Right: Average Levenshtein distances d_L of GPT-4o mini and TRECONLM on trace reconstruction for sequence length $L = 60$, using two, five, and ten noisy reads (right panel). GPT-4o mini is evaluated with zero-, three-, and five-shot prompting.

index. We then cap each cluster at a maximum of 10 reads to match TRECONLM’s context length. This results in 9,729 test examples.

Bar-Lev et al. [BL+25] report a failure rate of 0.146 for DNAformer, whereas TRECONLM achieves 0.111 with fewer reads and no dynamic-programming post-processing. While DNAformer was trained on synthetic data generated using error statistics derived from the real dataset, TRECONLM was pretrained on a fixed noise distribution and was not tuned to the Microsoft dataset. Thus, TRECONLM performs better under worse initial conditions.

C.3 GPT-4o mini

As an additional baseline, we compare TRECONLM to GPT-4o mini. We prompt GPT-4o mini as shown in Figure 12 to reconstruct sequences of length $L = 60$ using zero-, three-, and five-shot prompting. For TRECONLM, we use a 3M-parameter model with the same architecture as in Section C, trained on ~ 39.5 M examples with a compute budget of 6×10^{17} FLOPs. The dataset used here is larger than in Section C because of the shorter target length ($L = 60$ vs. 110).

We evaluate both models on 250 synthetic test instances per cluster size (2, 5, and 10), generated by the IDS channel with error probabilities drawn uniformly from $\mathcal{U}[0.01, 0.1]$. The few-shot examples shown to GPT-4o mini are sampled from the same distribution as the test set.

Figure 10, right panel, shows that TRECONLM achieves lower Levenshtein distances than GPT-4o mini across all tested cluster sizes.

D Baseline method parameters

We evaluate each baseline using the parameters specified in their original publications. When error probabilities p_I, p_D, p_S are required, we use estimates for the real datasets [Ant+20; Sri+21], and the mean values of the corresponding noise distributions for synthetic data, except for TrellisBMA at increased noise levels (Section 5.2.1). For TrellisBMA, we found that using the true mean values

at higher noise levels led to noticeably worse performance. Instead, we fixed the error parameters to the mean of the base noise distribution (corresponding to $k = 0$).

For BMALA and VS, we adopt the parameters from Sabary et al. [Sab+24]. BMALA uses a window size of $w = 3$. For the VS algorithm, we compute $\delta = (1 + p_S)/2$ and set $\gamma = 3/4$, $r = 2$, and $l = 5$.

For TrellisBMA, we use the same parameters as in Srinivasavaradhan et al. [Sri+21], setting $\beta_b = 0$ for all cluster sizes N from 2 to 10, and adapting β_e and β_i based on the cluster size. For cluster sizes $N \in \{2, 3\}$, we use $(\beta_e, \beta_i) = (0.1, 0.5)$; for cluster sizes $N \in \{4, 5\}$, $(1.0, 0.1)$; for cluster sizes $N \in \{6, 7\}$, $(0.5, 0.1)$; for cluster sizes $N \in \{8, 9\}$, $(0.5, 0.5)$; and for cluster size $N = 10$, $(0.5, 0.0)$.

For the two deep learning-based reconstruction methods, RobuSeqNet [Qin+24] and DNAFormer [BL+25], we adapt their data loaders to generate synthetic data according to the IDS channel, using the same noise distribution $\mathcal{U}(0.01, 0.1)$ as used for pretraining TReconLM.

The original implementations of RobuSeqNet [Qin+24] and DNAFormer [BL+25] apply learning rate annealing across epochs using cosine decay. Our adapted data loaders generate synthetic data dynamically at each iteration. We therefore train for a single epoch and adjust the learning rate schedule accordingly, using cosine decay with linear warm-up, as in TReconLM.

For RobuSeqNet, we increase the pretraining batch size to 1.5K for $L = 60$, 800 for $L = 110$, and 600 for $L = 180$ to accommodate larger compute budgets, using maximum learning rates of $\text{lr}_{\max} = 6.1 \times 10^{-4}$, 7.1×10^{-4} , and 9.7×10^{-4} , respectively (outperforming the default configuration of batch size 64 and learning rate 5×10^{-3}). For finetuning, we use a batch size of 8 for the Noisy DNA dataset and 52 for the Microsoft dataset, with a maximum learning rate of $\text{lr}_{\max} = 1 \times 10^{-5}$, as in TReconLM. All other hyperparameters follow the original implementation [Qin+24]. Dropout is set to 0.1 for the convolutional, RNN, and conformer-attention layers, and training uses the Adam optimizer with $\beta = (0.9, 0.98)$.

For DNAFormer [BL+25], we use the same configurations as in the original implementation. Training uses the Adam optimizer with $\text{lr}_{\max} = 3 \times 10^{-5}$, $\text{lr}_{\min} = 1 \times 10^{-7}$, a batch size of 64, $\beta = (0.9, 0.999)$, and no dropout or weight decay. We also experimented with larger batch sizes and scaled the learning rate accordingly, but this resulted in slightly worse performance. For finetuning, we set the batch size to 8 for the Noisy DNA dataset (with dropout set to 0.1) and 52 for the Microsoft dataset (with dropout kept at zero), using a maximum learning rate of $\text{lr}_{\max} = 1 \times 10^{-5}$.

E Attention matrix

To provide some interpretability into the underlying algorithm of TReconLM, we visualize the attention matrix of our pretrained 38M-parameter model. We consider sequences of length $L = 60$ and show a heatmap of the attention matrix for a prompt \mathbf{p} consisting of $N = 3$ reads. We plot the attention scores from the last layer using min-max normalization.

Figure 11 shows a diagonal structure, where read position j attends to sequence estimate position j . Earlier layers have broader attention patterns, where multiple read positions contribute to one sequence estimate position. This structure gradually becomes more focused across layers, resulting in the pattern shown in the final layer.

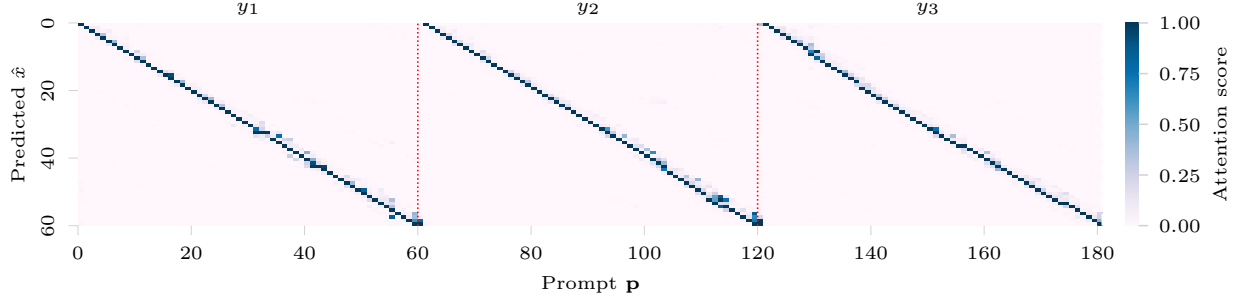


Figure 11: Visualization of the attention matrix for a prompt \mathbf{p} consisting of the concatenation of three traces, \mathbf{y}_1 , \mathbf{y}_2 , and \mathbf{y}_3 . Red lines indicate the ends of the traces.

F Proof of Proposition 1

The proof of Proposition 1 is relatively standard.

The logistic (population) risk is

$$R(\mathbf{w}) = \mathbb{E} \left[\ell(\mathbf{w}^T \mathbf{x}, y) \right],$$

where $\ell(z, y) = \log(1 + e^{-yz})$ is the logistic loss. The empirical risk of the examples is defined in Equation 3.

From [BJM06], we have that the 0/1-excess loss for \mathbf{w} is related to the logistic excess loss as follows: For any \mathbf{w} , we have that

$$\mathbb{P} \left[\text{sign}(\mathbf{w}^T \mathbf{x}) \neq y \right] - \mathbb{P} \left[\text{sign}(\mathbf{w}_B^T \mathbf{x}) \neq y \right] \leq 2(R(\mathbf{w}) - R(\mathbf{w}_*)). \quad (9)$$

where $\text{sign}(\mathbf{w}_B^T \mathbf{x})$ is the Bayes optimal classifier and \mathbf{w}_* is the optimal logistic classifier. Therefore, we have that

$$\mathbb{P} \left[\text{sign}(\hat{\mathbf{w}}^T \mathbf{x}) \neq y \right] \leq \mathbb{P} \left[\text{sign}(\mathbf{w}_B^T \mathbf{x}) \neq y \right] + 2(R(\hat{\mathbf{w}}) - R(\mathbf{w}_*)) \quad (10)$$

$$\leq e^{-2k(1/2-p)^2} + 4 \left(2 \frac{BR}{\sqrt{N}} + \sqrt{\frac{9 \log(2/\delta)}{2N}} \right), \quad (11)$$

where the last inequality holds with probability at least $1 - \delta$. Here, we used that the Bayes error probability is the probability that at least half of the entries were flipped and is bounded by

$$\mathbb{P} \left[\text{sign}(\mathbf{w}_B^T \mathbf{x}) \neq y \right] = \sum_{b=\lceil k/2 \rceil}^k \binom{k}{b} p^b (1-p)^{k-b} \leq e^{-2k(1/2-p)^2}.$$

Moreover, we used the following bound, proven below. With probability at least $1 - \delta$,

$$R(\hat{\mathbf{w}}) - R(\mathbf{w}_*) \leq 2 \left(2 \frac{BR}{\sqrt{N}} + \sqrt{\frac{9 \log(2/\delta)}{2N}} \right). \quad (12)$$

It remains to prove the bound (12).

We consider the function class

$$\mathcal{G} = \left\{ (\mathbf{x}, y) \mapsto \ell(\mathbf{w}^T \mathbf{x}, y) \mid \|\mathbf{w}\|_2 \leq B \right\}.$$

Thus, $z = y\mathbf{w}^T \mathbf{x}$ lies in the interval $[-BR, BR]$. Because of this bound, the logistic loss is bounded by

$$0 < \ell(z) = \log(1 + e^{-z}) \leq \log(1 + e^{BR}).$$

From a standard generalization bound based on the Rademacher complexity [BJM06], we get, for 1-Lipschitz loss and for all \mathbf{w} with $\|\mathbf{w}\|_2 \leq B$ that

$$\begin{aligned} R(\mathbf{w}) &\leq \hat{R}(\mathbf{w}) + 2r_N(\mathcal{G}) + \sqrt{\frac{9 \log(2/\delta)}{2n}} \\ &\leq \hat{R}(\mathbf{w}) + 2\frac{BR}{\sqrt{N}} + \sqrt{\frac{9 \log(2/\delta)}{2n}}, \end{aligned} \tag{13}$$

where r_N is the Rademacher complexity. For the second inequality, we used the bound $r_N(\mathcal{G}) \leq \frac{BR}{\sqrt{N}}$ on the Rademacher complexity of linear predictors.

We have that

$$R(\hat{\mathbf{w}}) = \hat{R}(\hat{\mathbf{w}}) + R(\hat{\mathbf{w}}) - \hat{R}(\hat{\mathbf{w}}) \tag{14}$$

$$\leq \hat{R}(\mathbf{w}_*) + R(\hat{\mathbf{w}}) - \hat{R}(\hat{\mathbf{w}}) \tag{15}$$

$$\leq R(\mathbf{w}_*) + 2 \left(2\frac{BR}{\sqrt{N}} + \sqrt{\frac{9 \log(2/\delta)}{2n}} \right), \tag{16}$$

where first inequality holds because $\hat{\mathbf{w}}$ minimizes the empirical risk, and therefore $\hat{R}(\hat{\mathbf{w}}) \leq \hat{R}(\mathbf{w}_*)$, and for the last equality, we applied the generalization bound (13) twice, once to bound $\hat{R}(\mathbf{w}_*)$, and once to bound $R(\hat{\mathbf{w}}) - \hat{R}(\hat{\mathbf{w}})$. This concludes the proof of the bound (12).

G Detailed numerical results

For better readability and comparison, we provide tables with the numerical results (Levenshtein distances and failure rates) for the experiments in the main paper. We include tables for the evaluation on IDS-generated data for $L = 110$ (Figure 2) and for real-world data experiments with the Noisy-DNA dataset (Figure 4) and the Microsoft dataset (Figure 5). Tables report results for both our pretrained and, for real-world datasets, fine-tuned models, as well as the considered baselines.

Table 2: Results for synthetic data of length $L = 110$ (see Figure 2).

Levenshtein distance d_L								
N	RobuSeqNet	VS	MUSCLE	BMALA	TrellisBMA	ITR	DNAformer	TReconLM
2	3.96e-1 (7.08e-2)	1.59e-1 (5.27e-2)	2.07e-1 (6.62e-2)	2.39e-1 (7.67e-2)	4.19e-1 (6.63e-2)	1.55e-1 (5.41e-2)	2.66e-1 (8.58e-2)	1.42e-1 (5.37e-2)
3	3.85e-1 (7.23e-2)	1.58e-1 (5.28e-2)	1.50e-1 (6.21e-2)	1.74e-1 (7.77e-2)	4.04e-1 (7.19e-2)	2.47e-1 (8.86e-2)	1.45e-1 (9.23e-2)	6.52e-2 (4.09e-2)
4	3.73e-1 (7.41e-2)	1.69e-1 (5.68e-2)	1.07e-1 (5.19e-2)	1.46e-1 (7.65e-2)	1.43e-1 (8.33e-2)	7.36e-2 (4.86e-2)	8.70e-2 (7.63e-2)	3.81e-2 (3.13e-2)
5	3.62e-1 (7.57e-2)	1.62e-1 (5.49e-2)	8.11e-2 (4.66e-2)	1.19e-1 (7.38e-2)	1.01e-1 (7.01e-2)	4.45e-2 (3.97e-2)	4.95e-2 (5.66e-2)	2.15e-2 (2.30e-2)
6	3.55e-1 (7.59e-2)	1.62e-1 (5.55e-2)	7.23e-2 (4.32e-2)	9.84e-2 (6.83e-2)	1.10e-1 (8.20e-2)	2.28e-2 (2.62e-2)	2.90e-2 (4.09e-2)	1.26e-2 (1.70e-2)
7	3.49e-1 (7.62e-2)	1.65e-1 (5.68e-2)	6.64e-2 (4.07e-2)	8.22e-2 (6.37e-2)	8.11e-2 (6.84e-2)	1.44e-2 (2.01e-2)	1.83e-1 (3.00e-2)	7.60e-3 (1.29e-2)
8	3.45e-1 (7.45e-2)	1.70e-1 (5.85e-2)	5.81e-2 (3.79e-2)	7.36e-2 (6.05e-2)	6.30e-2 (5.93e-2)	9.19e-3 (1.51e-2)	1.18e-2 (2.27e-2)	4.78e-3 (9.87e-3)
9	3.39e-1 (7.43e-2)	1.75e-1 (6.14e-2)	4.98e-2 (3.48e-2)	6.23e-2 (5.62e-2)	4.86e-2 (5.15e-2)	5.53e-3 (1.11e-2)	7.46e-3 (1.69e-2)	2.86e-3 (7.45e-3)
10	3.34e-1 (7.50e-2)	1.78e-1 (6.15e-2)	4.49e-2 (3.26e-2)	5.37e-2 (5.27e-2)	3.62e-2 (4.25e-2)	3.77e-3 (8.86e-3)	5.05e-3 (1.41e-2)	1.77e-3 (5.94e-3)
Failure rate								
N	RobuSeqNet	VS	MUSCLE	BMALA	TrellisBMA	ITR	DNAformer	TReconLM
2	1.00e+0	1.00e+0	1.00e+0	1.00e+0	1.00e+0	1.00e+0	1.00e+0	9.99e-1
3	1.00e+0	1.00e+0	9.99e-1	9.96e-1	1.00e+0	9.99e-1	9.73e-1	9.63e-1
4	1.00e+0	1.00e+0	9.94e-1	9.85e-1	9.88e-1	9.45e-1	8.97e-1	8.42e-1
5	1.00e+0	1.00e+0	9.79e-1	9.63e-1	9.62e-1	8.45e-1	7.67e-1	6.75e-1
6	1.00e+0	1.00e+0	9.71e-1	9.25e-1	9.50e-1	6.66e-1	6.22e-1	4.89e-1
7	1.00e+0	1.00e+0	9.64e-1	8.90e-1	9.01e-1	5.20e-1	4.80e-1	3.40e-1
8	1.00e+0	1.00e+0	9.44e-1	8.58e-1	8.58e-1	3.98e-1	3.83e-1	2.36e-1
9	1.00e+0	9.99e-1	9.17e-1	8.10e-1	7.85e-1	2.80e-1	2.61e-1	1.52e-1
10	1.00e+0	9.99e-1	9.00e-1	7.65e-1	7.06e-1	2.12e-1	1.88e-1	9.67e-2

Table 3: Results for Noisy-DNA dataset (see Figure 4). Pretrained models (p) and finetuned models (f).

Levenshtein distance d_L							
N	VS	MUSCLE	BMALA	TrellisBMA	ITR	TReconLM (p)	TReconLM (f)
2	3.88e-1 (1.75e-1)	4.32e-1 (1.32e-1)	4.38e-1 (1.15e-1)	5.40e-1 (1.08e-1)	3.78e-1 (1.77e-1)	3.84e-1 (1.41e-1)	3.25e-1 (1.96e-1)
3	3.88e-1 (1.69e-1)	4.20e-1 (1.39e-1)	4.16e-1 (1.20e-1)	5.30e-1 (1.08e-1)	5.68e-1 (1.44e-1)	3.54e-1 (1.45e-1)	3.01e-1 (2.02e-1)
4	3.95e-1 (1.58e-1)	3.70e-1 (1.41e-1)	3.97e-1 (1.23e-1)	4.50e-1 (2.03e-1)	3.77e-1 (1.62e-1)	3.23e-1 (1.55e-1)	2.70e-1 (2.10e-1)
5	3.88e-1 (1.62e-1)	3.59e-1 (1.40e-1)	3.88e-1 (1.24e-1)	4.10e-1 (2.01e-1)	3.70e-1 (1.70e-1)	3.09e-1 (1.54e-1)	2.48e-1 (1.51e-1)
6	3.87e-1 (1.61e-1)	3.53e-1 (1.41e-1)	3.78e-1 (1.30e-1)	4.37e-1 (2.09e-1)	3.22e-1 (1.73e-1)	2.95e-1 (1.55e-1)	2.30e-1 (2.14e-1)
7	3.79e-1 (1.62e-1)	3.47e-1 (1.42e-1)	7.58e-3 (1.30e-1)	4.00e-1 (2.15e-1)	3.03e-1 (1.77e-1)	2.79e-1 (1.54e-1)	2.10e-1 (2.11e-1)
8	3.81e-1 (1.58e-1)	3.35e-1 (1.45e-1)	3.59e-1 (1.30e-1)	3.14e-1 (1.86e-1)	2.83e-1 (1.77e-1)	2.68e-1 (1.56e-1)	2.00e-1 (2.12e-1)
9	3.82e-1 (1.56e-1)	3.23e-1 (1.44e-1)	3.51e-1 (1.30e-1)	3.00e-1 (1.88e-1)	2.74e-1 (1.77e-1)	2.62e-1 (1.55e-1)	1.78e-1 (2.09e-1)
10	3.72e-1 (1.56e-1)	3.13e-1 (1.47e-1)	3.40e-1 (1.33e-1)	3.32e-1 (2.59e-1)	2.60e-1 (1.78e-1)	2.54e-1 (1.55e-1)	1.68e-1 (2.08e-1)
Failure rate							
N	VS	MUSCLE	BMALA	TrellisBMA	ITR	TReconLM (p)	TReconLM (f)
2	9.94e-1	9.99e-1	1.00e+0	1.00e+0	9.94e-1	1.00e+0	9.84e-1
3	9.93e-1	9.99e-1	1.00e+0	1.00e+0	1.00e+0	9.99e-1	9.57e-1
4	9.97e-1	9.97e-1	1.00e+0	9.97e-1	9.92e-1	9.99e-1	9.32e-1
5	9.94e-1	9.98e-1	1.00e+0	9.97e-1	9.88e-1	9.99e-1	9.00e-1
6	9.98e-1	9.95e-1	1.00e+0	9.95e-1	9.80e-1	1.00e+0	8.60e-1
7	9.96e-1	9.96e-1	1.00e+0	9.93e-1	9.65e-1	9.99e-1	8.26e-1
8	9.96e-1	9.92e-1	1.00e+0	9.90e-1	9.73e-1	1.00e+0	7.82e-1
9	9.97e-1	9.92e-1	1.00e+0	9.88e-1	9.63e-1	9.99e-1	7.40e-1
10	9.95e-1	9.93e-1	1.00e+0	9.88e-1	9.60e-1	1.00e+0	6.74e-1

Table 4: Results for Microsoft dataset (see Figure 5). Pretrained models (p) and finetuned models (f).

Levenshtein distance d_L							
N	VS	MUSCLE	BMALA	TrellisBMA	ITR	TReconLM (p)	TReconLM (f)
2	5.78e-2 (2.96e-2)	6.65e-2 (3.10e-2)	1.23e-1 (6.56e-2)	1.85e-1 (8.56e-2)	5.31e-2 (3.06e-2)	5.28e-2 (2.08e-1)	3.90e-2 (2.80e-2)
3	5.78e-2 (3.08e-2)	4.85e-2 (2.46e-2)	5.15e-2 (4.03e-2)	1.60e-1 (7.85e-2)	9.13e-2 (4.15e-2)	1.43e-2 (2.17e-1)	1.09e-2 (1.55e-2)
4	7.30e-2 (1.36e-2)	0.252 (5.33e-2)	4.10e-2 (3.47e-2)	1.59e-2 (1.68e-2)	8.99e-3 (1.21e-2)	7.93e-3 (1.90e-1)	4.53e-3 (9.78e-3)
5	6.44e-2 (4.54e-2)	9.02e-3 (1.04e-2)	2.70e-2 (2.91e-2)	1.02e-2 (1.42e-2)	5.06e-3 (8.87e-3)	4.26e-3 (1.37e-1)	2.17e-3 (6.97e-3)
6	6.18e-2 (3.89e-2)	8.34e-3 (9.44e-3)	2.16e-2 (2.70e-2)	6.84e-3 (1.15e-2)	3.11e-3 (6.57e-3)	3.27e-3 (1.35e-1)	1.35e-3 (5.04e-3)
7	6.17e-2 (4.08e-2)	9.05e-3 (9.53e-3)	1.61e-2 (2.31e-2)	5.06e-3 (9.38e-3)	1.96e-3 (5.11e-3)	1.86e-3 (1.20e-1)	7.91e-4 (3.61e-3)
8	6.44e-2 (4.90e-2)	4.73e-3 (6.77e-3)	1.37e-2 (2.01e-2)	4.61e-3 (9.36e-3)	1.65e-3 (4.43e-3)	1.51e-3 (1.08e-1)	6.64e-4 (3.59e-3)
9	6.78e-2 (4.76e-2)	3.13e-3 (5.56e-3)	1.08e-2 (2.00e-2)	3.40e-3 (8.96e-3)	1.34e-3 (4.20e-3)	1.34e-3 (9.17e-2)	4.20e-4 (2.73e-3)
10	7.26e-2 (4.96e-2)	3.29e-3 (5.51e-3)	9.05e-3 (1.45e-2)	4.60e-3 (8.59e-3)	1.63e-3 (4.05e-3)	1.16e-3 (1.05e-1)	3.90e-4 (2.54e-3)
Failure rate							
N	VS	MUSCLE	BMALA	TrellisBMA	ITR	TReconLM (p)	TReconLM (f)
2	9.80e-1	9.92e-1	9.95e-1	9.99e-1	9.61e-1	9.68e-1	8.73e-1
3	9.70e-1	9.82e-1	9.01e-1	9.89e-1	9.79e-1	6.06e-1	4.29e-1
4	9.66e-1	7.25e-1	8.65e-1	6.34e-1	4.49e-1	4.08e-1	2.21e-1
5	9.71e-1	5.53e-1	6.90e-1	4.45e-1	3.16e-1	2.26e-1	1.09e-1
6	9.66e-1	5.65e-1	6.16e-1	3.28e-1	2.21e-1	1.89e-1	8.05e-2
7	9.74e-1	5.96e-1	5.00e-1	2.67e-1	1.54e-1	1.04e-1	4.78e-2
8	9.45e-1	3.81e-1	4.93e-1	2.50e-1	1.42e-1	8.85e-2	3.54e-2
9	9.58e-2	2.66e-1	3.76e-1	2.18e-1	1.06e-1	7.62e-2	2.31e-2
10	9.69e-1	2.89e-1	3.65e-1	2.14e-1	1.56e-1	7.29e-2	2.35e-2

Example prompt for GPT-4o mini:

We consider a reconstruction problem of DNA sequences. We want to reconstruct a DNA sequence consisting of 60 characters (either A,C,T or G) from 5 noisy DNA sequences. These noisy DNA sequences were generated by introducing random errors (insertion, deletion, and substitution of single characters). The task is to provide an estimate of the ground truth DNA sequence.

Here are some examples:

Example #1

Input DNA sequences:

1. GATACGGATTGTGCTCGAGTGGATACTGGTATAGAGAAGAGAGTAATGCTAAGGTAG
2. ATATAGGACTGTTCCCTCGAAGTGGATACTGTACAAAAATCAGAAGCGAGTAAGGTAG
3. GATCAGGATTGTACTCGAGTGTCTACTGTACAAAGCGTCAGAGGTGCCATAGGTACG
4. GATAAAGGGACGTTGCCCGAGTGATACTGTCAAAGCGTAAAAGAGATGCTAGGTG
5. GGATCAAGGATTGCTTGTCGAGTGTGATACTGTACAATGATCAGAAGAGATTAATAG

Correct output:

GATAAAGGATTGTTGCTCGAGTGGATACTGTACAAAGAGTCAGAAGAGATGCTAAGGTAG

Example #2

Input DNA sequences:

1. AAACCCTTACGGGTCGAATACATCTTATCCGAGCGCCTCAAGGAGTAGCGATTCCTAC
2. AAACCCATAGGGTCCAAAAATATTTACCGTGCACTCCGAAAGGGAGTATCGTTGATA
3. AAACACTTGGGGTCGAAAAAATACTATCCGTGTACCCCAGAGGTGTAGTGTCTCATAC
4. AACCTGAGGGTCGAAACTGTTGATCCGTGCACCTCATGAGGGTGTGCGGGCATGC
5. AAACCTTAGGGCTCGAATACATATTTACCGTGACCTCCAGAGGAGTAGCGTTTCAA

Correct output:

AAACCCTTAGGGTTCGAATACATATTTATCCGTGCACCTCCAGAGGAGTAGCGTTTCATAC

Example #3

Input DNA sequences:

1. TGCCCCGACGATATGCCGGCGGATACACTCTCACGATCGTCAAGTATATCCGTTAA
2. ATGCCCGACGCTTCTGGCCGGATACACTCAACAATCGTCACCGTTTATCCGATAA
3. ATGCCCGACGAATGCTGGCCGGATACACTTACACGATGTCAATGATATCCGAGTG
4. ATGCCACGAGTATGCTGCCGGATCCTCACAAATCGTCAAGTTATATCCCGATAT
5. ATGCCCGATAATATATGGCCGACTCCACTCTACACGTCGTCAAGTTATATCCCGTTAG

Correct output:

ATGCCCGACGATATGCTGGCCGGATACACTCTACACGATCGTCAAGTTATATCCCGTTAT

Task:

Reconstruct the DNA sequence from the following noisy input sequences.

Input DNA sequences:

1. GGTCCCTAGAAGGATTGGATGCTGTTGCGGGGTATCTAATGTTGTGCCTTGGTGCAT
2. AGGTGCGCCAGAAGTGATATGGTCGCTGGCGCGGCATCTAATTTGTGACATCTTGAT
3. AGGTTACCCTGATAGTGATGTAGTGTGCATTTGCGGGCTCTATGTTGTGCCTGTTGCT
4. AGGTCCTAGTAAGGTATATGCATGCGGTGCGGGCTCTAATGTTGTGCTTGAGTTGCT
5. AGCTCCGTAGAGGAATGATGCTGTTGCGCCGGCATTAGATGTGTGCCTCGGTTGCT

Provide an estimate of the ground truth DNA sequence consisting of 60 characters in the format ***estimated DNA sequence*** - use three * on each side of the estimated DNA sequence.

Figure 12: Three-shot prompt example for GPT-4o mini.